Energy & Environmental Science

Accepted Manuscript

ROYAL SOCIETY OF CHEMISTRY

www.rsc.org/ees

Energy &Environmental Science

COMMUNICATION

Bioinspired Piezoelectric Nanogenerators Based on Vertically Aligned Phage Nanopillars†

Received 00th January 20xx,
Accepted 00th January 20xx

DOI: 10.1039/x0xx00000x

www.rsc.org/

Dong-Myeong Shin[a‡], Hye Ji Han[b‡], Won-Geun Kim[a], Eunjong Kim[c], Chuntae Kim[a], Suck Won Hong[d], Hyung Kook Kim[a,b,c], Jin-Woo Oh[a,b,c,*] and Yoon-Hwae Hwang[a,b,c,*]

Bioinspired nanogenerators based on vertically aligned phage nanopillars are inceptively demonstrated. Vertically aligned phage nanopillars enable not only a high piezoelectric response but also a tuneable piezoelectricity. Piezoelectricity is also modulated by tuning of the protein's dipoles in the each phage. The sufficient electrical power from phage nanopillars thus holds promise for the development of self-powered implantable and wearable electronics.

Currently, medically implantable devices, including pacemakers, deep brain stimulators and neural stimulators, require a rechargeable battery to avoid expensive and risky surgery for replacing the consumed battery. Piezoelectric nanogenerators composed of organic[1] and inorganic materials[2] have been developed to utilize the mechanical energy in a human body to sustainably power an implantable device. Due to their non-toxicity and biocompatibility, fibrous nature materials, such as collagen fibril,[3] peptide fibril[4] and bacteriophages,[5] have attracted considerable attention as promising piezoelectric materials. Although these materials exhibit a strong piezoelectric response in the axial direction rather than radially,[6] the realization of a vertically aligned one-dimensional structure is still a significant challenge due to the limpness and pliableness of fibrous nature materials. Here, we demonstrate vertically aligned M13 bacteriophage (phage) nanopillars (Fig. 1) using enforced infiltration. We then characterize the axial piezoelectric response of the resulting phage nanopillars (PNPs) and use them to develop a PNP-based nanogenerator. The vertically aligned PNP-based nanogenerator exhibits electrical output that is up to ~2.6-fold higher than that of the laterally assembled phage-based nanogenerator, likely due to the higher elasticity in the axial direction. The PNP-based nanogenerator can be useful for numerous bio-implantable and wearable electronics applications because phages are self-replicable and environmentally friendly materials.

As a building block for fibrous piezoelectric material, we have chosen a bacterial virus, the M13 bacteriophage (phage). Phages that have well-defined structural features and narrow size distribution can easily produce a million identical copies by infecting the bacterial host cells. Viral particles have previously been used to create functional nanomaterials for energy harvesting[7] and storage,[8] chemical sensors[9] and semiconducting nanomaterial synthesis and assembly.[10] The M13 bacteriophage is a filamentous bacterial virus composed of single-stranded DNA, which is covered by 2,700 copies of the major coat protein (pVIII) and capped with five copies of minor coat proteins (pIII/pVI and pVIII/pIX) on either end. The pVIII proteins have an α-helix structure with a dipole moment directed toward the anchoring domain and are arranged with a combined five-fold rotational and two-fold screw symmetry (Fig. 1). A net dipole moment of pVIII proteins leads to a permanent polarization in an axial direction of the phage; thus, we expect piezoelectricity from the vertically aligned phages. Furthermore, we expect a high piezoelectric response compared

Broader context

Energy harvesting from mechanical resources has attracted great attentions owing to the demands for a power supply of implantable and wearable electronics, operated in the power range of microwatt to nanowatt. Biomaterials have attracted great attentions as promising materials for energy harvesting owing to their non-toxicity and biocompatibility. M13 bacteriophages are relevant in this context because we can easily modulate their functions through genetic engineering. In this contribution, we show that M13 bacteriophage nanopillars work as efficient piezoelectric material and thereby can be used to provide the functional material in energy harvesting devices. The sufficient electrical power from phage nanopillars thus holds promise for the development of self-powered implantable and wearable electronics. The apparent versatility of M13 bacteriophage also suggests that phage nanopillars can serve as functional nanomaterials for numerous electronic and optoelectronic applications.

[a] Department of Nano Fusion Technology & BK21 Plus Nanoconvergence Technology Division, Pusan National University (PNU), Busan 46241, Republic of Korea, E-mail: ojw@pusan.ac.kr (J.-W. Oh), yhwang@pusan.ac.kr (Y.-H. Hwang)
[b] Department of Advanced Circuit Interconnection, Pusan National University (PNU), Busan 46241, Republic of Korea
[c] Department of Nano Energy Engineering, Pusan National University (PNU), Busan 46241, Republic of Korea
[d] Department of Cogno-Mechatronics Engieering, Pusan National University (PNU), Busan 46241, Republic of Korea

† Electronic Supplementary Information (ESI) available: Detailed experimental methods and supplementary data. See DOI: 10.1039/x0xx00000x

‡ These authors contributed equally to this work.

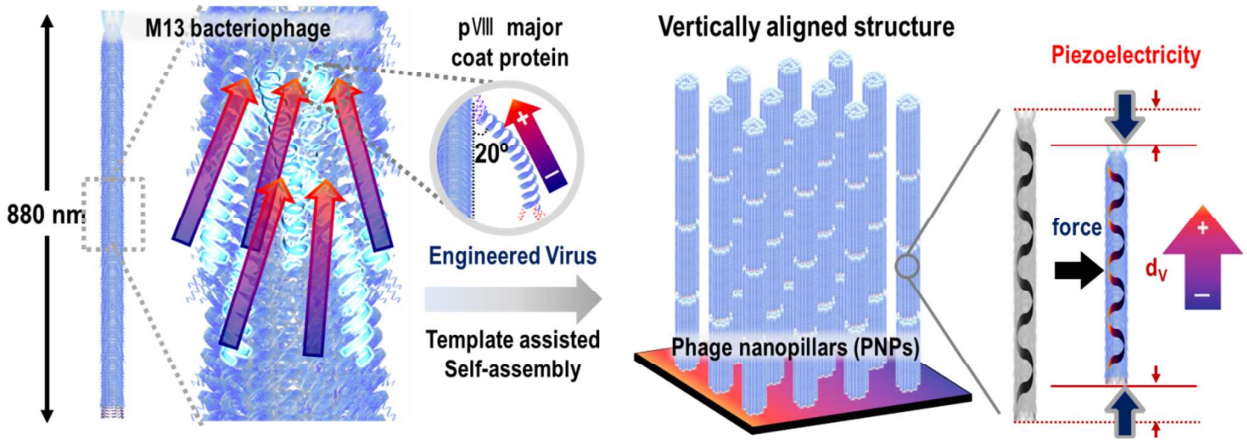

Fig. 1. Schematic of vertically aligned M13 bacteriophage nanopillars. The M13 bacteriophage has a well-defined structure with a length of 880 nm and a diameter of 6.6 nm and is covered by approximately 2,700 copies of the major coated protein (pVIII). The pVIII proteins are arranged with five-fold rotational and two-fold screw symmetry. Because each pVIII has a dipole moment that is directed from the tail (blue) to the anchoring domain (red), a net polarization points from the pIX protein (grey) to the pIII protein (cyan). The rainbow arrow indicates the dipole direction. b) Schematic of a single pVIII major coated protein. The pVIII protein is anchored to the single-stranded DNA with a tilt angle of 20°. The rainbow arrow indicates the dipole direction that is directed from the N-terminus to the C-terminus. The vertically aligned M13 bacteriophages, which were termed the phage nanopillars, were successfully fabricated using template-assisted self-assembly. The resulting structure exhibited piezoelectricity due to the deformation of the phage nanopillars in the axial direction.

to laterally assembled phages due to the high elasticity property along the axial direction of DNA.[11]

We first assembled the vertically aligned phages by building an apparatus to extrude the phage suspension into a porous template at precisely controlled speeds (Fig. 2a). As the suspensions were enforcedly infiltrated into a template, negatively charged phages are randomly adsorbed on the positively charged inner surface of the porous template (isoelectric point = 8-9) by electrostatic interaction. Then, the directional flow of the suspension and the liquid-crystalline property induced a spontaneous assembly process on the surface. As the infiltrations were repeated, the phages were consecutively trapped on the inner surface of the template, leading to the complete accumulation and deposition of the phages on the fluted channels in the porous template (Fig. 2b), which we termed phage nanopillars (PNPs). After a single cycle of enforced infiltration, the porous template outlet was completely packed with phages, as shown in Fig. S1. Using energy-dispersive X-ray spectroscopy (EDS, Fig. S2), we confirmed that the carbon and nitrogen concentrations in the porous channel increased considerably when it progressed from inlet to outlet, indicating that phages were successfully adsorbed on the porous template with the director along the direction of the template's channel. In addition, we can still find densely packed phage bundles in the porous template after the template was dissolved in a 0.5 M H_3PO_4 aqueous solution at the regulated reaction time (Fig. 2c). To better visualize the PNP structures in the porous template, PNPs were embedded in a polydimethylsiloxane (PDMS) supporter, and the porous template was completely dissolved as previously described (Fig. S3). Although scanning electron microscopy (SEM) images illustrate that phage bundles were flabbily lying on a substrate after removal of the porous template, noticeable phage bundle structures were observed.

The heights of PNPs (Fig. 2d-f and Fig. S4) could be tuned by varying parameters such as the phage concentration used for infiltration and the cycles of consecutive infiltration at a constant extrusion speed of 70 μL min^{-1}. The average height of PNPs increased with the number of infiltration cycles, whereas increasing the phage concentration caused the height to decrease. A high phage concentration (0.3 mg mL^{-1}) resulted in the lowest filling rate of 2.5 ± 0.5μm $cycle^{-1}$, with an increase in filling rate for each decrease in phage concentration down to 0.05 mg mL^{-1}, which exhibited the highest rate of 6.6 ± 0.7μm $cycle^{-1}$ (Fig. S5). We then calculated the adsorbed rates of phages on the porous template using the concentration of the extruded phage suspension (Fig. S6). The results indicated an increased adsorption rate with decreasing phage concentration up to the highest value of 0.1 mg $cycle^{-1}$ for a phage concentration of 0.05 mg mL^{-1}. A high phage concentration enables the formation of a phage clot in a confined geometry, and phage clots in enforced flows most likely pushed the adsorbed phages out of the porous template. Alternately, freely floating phages at low concentrations passed though the adsorbed phages on the porous template, allowing the unbounded phage suspension to leave the porous template freely. As a result, we successfully fabricated height-tuneable PNPs in the porous membrane by controlling each parameter that affects the kinetics of the enforced infiltration.

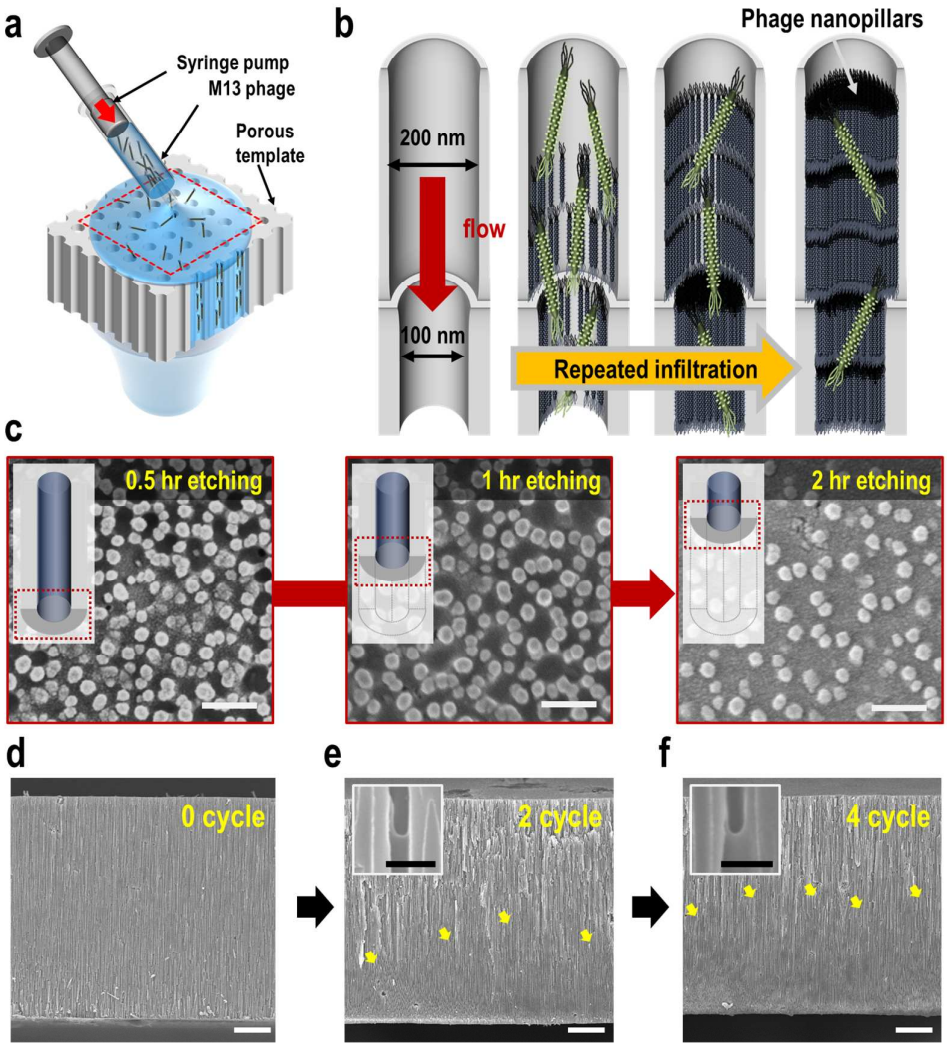

Fig. 2. Fabrication and structural modulation of phage nanopillars. a)Schematic of the enforced infiltration for the assembly of the vertically aligned M13 bacteriophages (phages), termed the phage nanopillars. b) Schematic illustration of the phage nanopillar formation controlled by repeated infiltration in the porous template. Consecutive enforced infiltration results in the porous channels being closely packed with phage bundles, which we termed phage nanopillars. c) SEM images of the phage nanopillar-embedded porous template that was dissolved in 0.5M H_3PO_4 at the regulated etching time (30 min to 2 h). Porous channels were fully filled with phage bundles after a sufficient amount of etching, indicating that phage nanopillars were successfully formed in the porous template. Scale bar = 200 nm. d,e,f) Cross-sectional view of the phage nanopillars in the porous template at different infiltration cycles. The average height of the phage nanopillars increased with increasing infiltration cycle. Yellow arrows indicate successfully formed phage nanopillars in the porous template. Insets in e) and f) represent the boundaries between the filled and empty regions. Scale bar = 10 μm. Scale bar in inset = 500 nm.

To verify the piezoelectric response of the resulting PNPs in the porous template, we monitored the mechanical response while applying an electrical signal through a metal-coated atomic force microscope (AFM) tip (Fig. 3 and Fig. S7). To characterize the axial piezoelectric properties, the gold electrode was thermally deposited on the single face of the porous template that included the PNPs. The AFM topography image in Fig. 3a represents the typical morphology of the porous template with a regular pore distribution and uniform pore size of ~200 nm. The piezoresponse force microscopy (PFM) image in Fig. 3b shows the characteristic bright and dark porous textures. Potential and height profiles in given areas, depicted in Fig. 3a and 3b, reveal that PNPs in pores responded to an applied electric field (Fig. 3c). These responses demonstrated the existence of axial piezoelectricity, presumably due to the compressive deformation of PNPs in the axial direction under an electric field. Then, we identified the piezoelectric response of PNPs along and across the porous

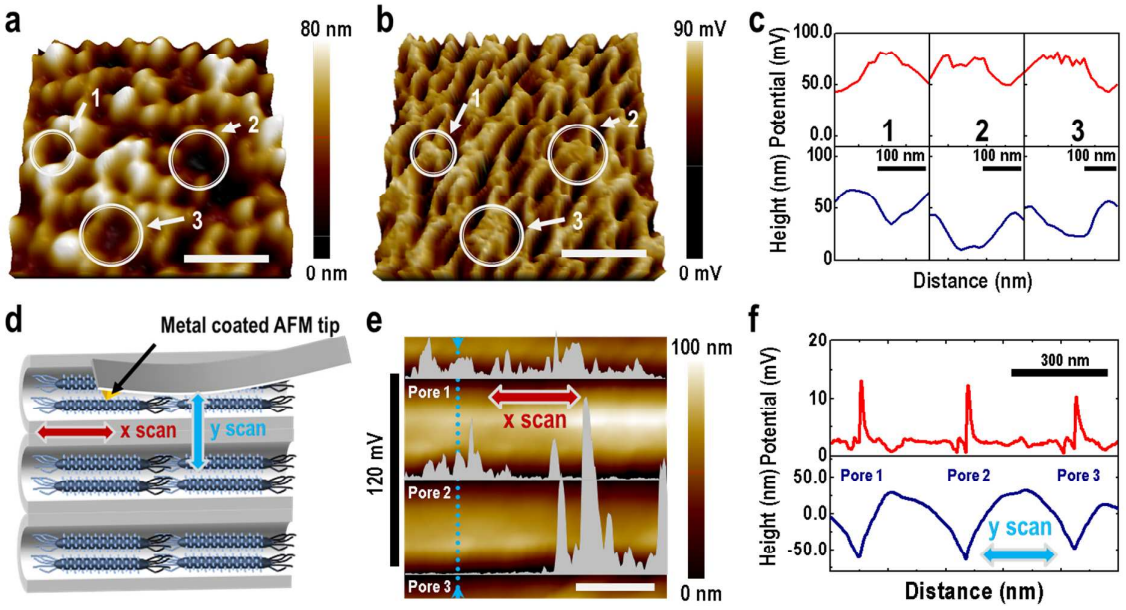

Fig. 3. Piezoelectric responses of phage nanopillars. a,b)AFM topography (a) and corresponding PFM image (b) of phage nanopillars in the porous template. Scale bar=300 nm. c) Potential (top) and height (bottom) profile of phage nanopillars in a given area (depicted in a and b). The potential in the groove regions was higher than that in ridge regions, indicating that the phage nanopillars in the pore exhibited piezoelectricity. d) Schematic of the PFM measurement for phage nanopillars in the porous channel. PFM responses were measured using the lateral PFM mode with two independent probing directions (x and y scans). e) AFM image of the porous template that includes the phage nanopillars in the cross-sectional view. Scale bar=300 nm. The series of line profiles of the potential output signal when the AFM tip scanned a cross-sectional porous template along the axial directions of the phage nanopillars. When probing along the axial direction of phage nanopillars (X_1,X_2,X_3), we observed a potential gradient because the dipole orientation was parallel to the scan direction. f) The PFM signals were obtained along radial (Y) directions of the phage nanopillars (measured lines were depicted in e). The piezoelectric response was independent of the scan direction when we scanned along the radial direction of the phage nanopillars.

channel (Fig. 3d). The AFM image in Fig. 3e shows the periodic dark fringes with a band spacing of ~200 nm. The corresponding output voltage image was recorded simultaneously when the AFM tip was scanned either along the porous channel (X_1, X_2, X_3) or across the porous channel (Y) (Fig. 3f). When we performed PFM measurement along the long axes of the PNPs (X_1, X_2, X_3), we observed the potential gradient along the axial direction of the PNPs. This gradient is likely the result of the aligned dipole moment along the axial direction of the PNPs, which causes a potential difference when probing PNPs that are oriented parallel to the scan direction. When scanning across the porous channel (Y), the piezoelectric response exhibits a ridge and groove band pattern. Because the radial dipole moment of the PNPs is independent of the probing orientation,[5] the observed piezoelectric response represented a similar potential at the ridge region. These results provide both compressive and shear piezoelectricity of the PNPs in the porous channel.

We constructed the PNP-based piezoelectric nanogenerators using vertically aligned phages in the porous template. Infiltrated PNPs in porous templates acted as a piezoelectric material, and the top and bottom electrodes were deposited on both surfaces of the porous templates using a thermal evaporator (Fig. 4a). The nanogenerators were encapsulated by a PDMS elastomeric layer that provided high structural stability, including durability and robustness. The electrical outputs were measured by applying the periodic compressive loads using a programmed linear motor. When applying a compressive load perpendicular to a nanogenerator that included PNPs of ~50.1μm, the output voltage reached up to ~200 mV with a decay time constant of ~0.04 s, and the output current was observed to reach ~13 nA under an applied load of F=30 N (Fig. S8). The charge value was extracted from the integration of a single current peak, Q~182 pC, and then, we estimated the piezoelectric coefficient as d_{33}= 6.1±0.1 pmV^{-1} using the relation for the quasi-static piezoelectric coefficient $d_{33}=Q/F$.[12] Polarity switching tests indicated an opposite output signal when the device was reversely connected, suggesting that the output electrical signals came from the PNPs, not from contact electrification between the measurement set-up and device. We then investigated the effect of infiltration cycles on the electrical outputs (Fig. 4b and 4c); the electrical outputs increased linearly from the 1st to 7th infiltration cycles. The output voltage and current could be increased to ~140.8 mV and ~9.5 nA, respectively. For a constant strain of PNPs, a potential drop along the PNPs can be approximated by

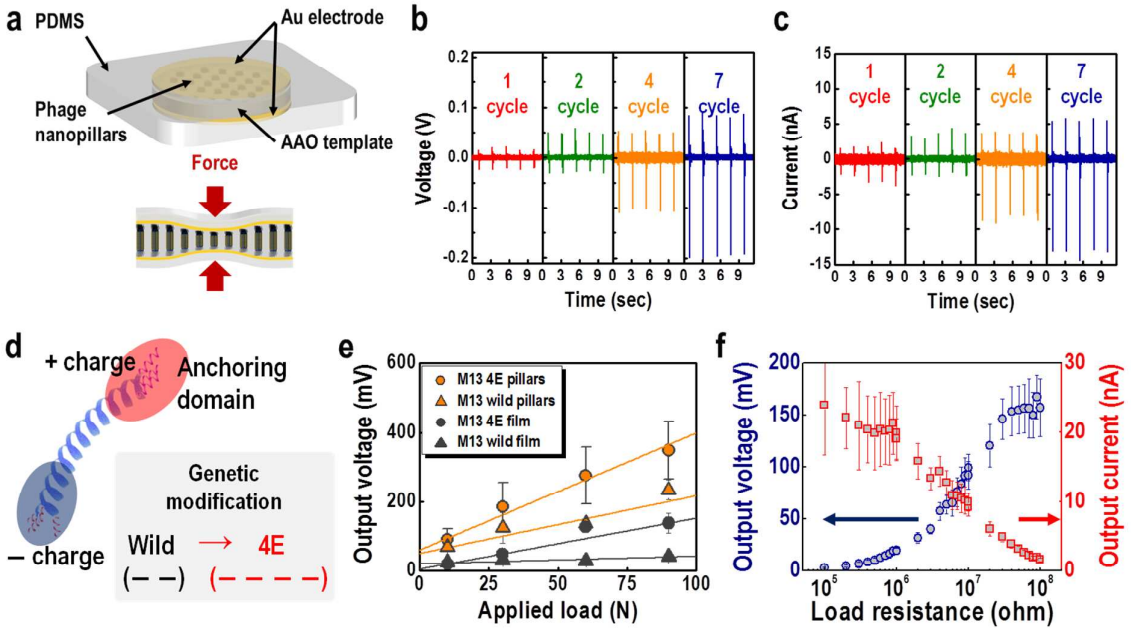

Fig. 4. Characterization of the phage nanopillar-based nanogenerator. a) Schematic of a phage nanopillar nanogenerator. A periodic external force was applied to the nanogenerator. b,c) Output voltages (b) and current (c) from the wild phage nanopillar-based nanogenerator that was prepared via controlled infiltration cycles (1 to 7). Electrical outputs increased with an increasing number of infiltration cycles. d) Schematic representation of a single pVIII major coated protein that is genetically engineered to modulate the dipole strength. The dipole strength can be modified by modulating the number of glutamates between the first and fifth amino acids in the tail region. e) Comparison of the load-dependent output voltages of the phage nanopillar-based nanogenerator with those of the phage film-based nanogenerator. f) Output voltage and current from the 4E phage nanopillar-based nanogenerator as a function of different resistors as external loads.

$\Delta V=\varepsilon_z e_{33} H$, where ε_z is the strain, e_{33} is the piezoelectric tensor and H is the height of the PNPs.[13] Based on this relationship, we successfully modulated the piezoelectric performance of the nanogenerator by regulating the PNP height using controlled infiltration (Fig. S9). To further investigate the output power from the piezoelectric nanogenerator that was produced through the 7 infiltration cycles, the different resistors were used as an external load (Fig. S10). The current amplitude gradually decreased with increasing external load due to the ohmic loss, whereas the output voltage exhibited an opposite trend. The corresponding output power reaches a maximum of ~0.3 nW at an external resistance of ~10 MΩ, indicating that an internal resistance is matched to external load.

To enhance the piezoelectric performance of virus-based piezoelectric nanogenerators, phages were engineered with four negatively charged glutamates (E) using a recombinant DNA technique (Fig. 4d). Four glutamates (4E) were substituted for alanine (A) in the aspartate (D) amino acid between the first (alanine) and fifth (aspartate) amino acids of the major coated protein pVIII in a wild-type phage, causing an increase in a dipole moment of the pVIII protein (the protein sequences are shown in Fig. S11). The piezoelectric nanogenerator was prepared with the engineered 4E phage nanopillars (4E PNPs), as described previously. The 4E PNPs-based nanogenerator produced an average output voltage and current of 232 mV and 11.1 nA (Fig. S12), respectively, and these results showed that the electrical outputs were improved by ~2-fold compared to those associated with the wild PNPs-based nanogenerator. The output voltage increased linearly for applied loads from 10 to 90 N (Fig. 4e), and we were able to increase the voltage output up to ~349 mV. We also approximated the piezoelectric coefficient from the integral of the single current peak at the applied load of F=30N (Fig. S13). The 4E PNPs exhibited a d_{33} value of 10.4±0.5 pm V^{-1}. We also compared the piezoelectric response of the PNPs-based nanogenerator with that of the laterally assembled phages (phage film-based nanogenerators, wild phage film and 4E phage film; for detailed procedures, see the ESI). Interestingly, PNPs-type phages exhibited a d_{33} value that was approximately 3-fold higher than that of the film-type phages. A piezoelectric response in the axial direction mainly corresponds to compressive deformation of DNA in the M13 bacteriophage; thus, the considerably higher electrical performance for the PNPs-based nanogenerator is presumably due to the high elasticity of DNA in the axial direction.[11] Then, the maximum peak power of the 4E PNPs-based nanogenerator was investigated using different resistors, with a value of 0.99 nW at a load resistance of ~10 MΩ (Fig. 4f and Fig. S14), which was ~3-fold more than that of the wild PNPs, as expected, because of charge distribution in 4E-type pVIII major coat protein. Finally, we lit up a liquid crystal display to demonstrate the power output of our nanogenerator (Video S1 and Fig. S15).

Conclusions

We have demonstrated height-tuneable vertically aligned phage nanopillars through enforced infiltration and the piezoelectric response of the resulting materials. Vertically aligned PNPs enable a high piezoelectric response and tuneable piezoelectricity. Furthermore, our approach to fabricate vertically aligned PNPs provides multiple advantages for numerous functional materials. First, we can easily fabricate vertically aligned long PNPs of bioinspired materials with a tuneable height through enforced infiltration. Second, we can easily produce scaled-up PNPs using a large-area porous template. The two-step anodization process enables the simple production of a large-scale well-ordered porous template.[14] Moreover, we can modulate the functions of the phage through genetic engineering. Thus, PNPs can be functional nanomaterials for numerous electronic and optoelectronic applications, such as lithium ion batteries, dye-sensitized solar cells and biosensors. In addition to the apparent versatility of the enforced infiltration methodology, the sufficient power of the PNP-based nanogenerator suggests feasible applications for either power supplies or strain sensors of small electronics. Further development and tuning of the structural protein's dipoles in the virus hold promise for the development of self-powered implantable[15] and wearable electronics.[16]

Acknowledgements

This work was supported by a National Research Foundation of Korea (NRF) grant funded by the Korean government (MSIP) (No.2014R1A2A1A11051146). This research was also supported by the Pioneer Research Center Program (2013M3C1A3065525) through the National Research Foundation of Korea, which is funded by the Ministry of Science, ICT & Future Planning.

References

1 (a) M. Lee, C. –Y. Chen, S. Wang, S. N. Cha, Y. J. Park, J. M. Kim, L. –J. Chou and Z. L. Wang, *Adv. Mater.,* 2012, **24**, 1759; (b) J. –H. Lee, K. Y. Lee, M. K. Gupta, T. Y. Kim, D. –Y. Lee, J. Oh, C. Ryu, W. J. Yoo, C.-Y. Kang, S. –J. Yoon, J.-B. Yoo and S. W. Kim. *Adv. Mater.,* 2014, **26**, 765; (c) W. –S. Jung, M. –G. kang, H. G. Moon, S. –H. Baek, S. –J. Yoon, Z. –L. Wang, S. –W. Kim and C. –Y. Kang, *Scientific Report*s, 2015, **5**, 9309.

2 (a) J. M. Wu, C. Xu, Y. Zhang and Z. L. Wang, *ACS Nano,* 2012, **6**, 4335; (b) T. T. Pham, K. Y. Lee, J. –H. Lee, K. –H. Kim, K. –S. Shin, M. K. Gupta, B. Kumar and S. –W. Kim, *Energy Environ. Sci.,* 2013, **6**, 841; (c) Y. Hu, L. Lin, Y. Zhang and Z. L. Wang, *Adv. Mater.,* 2012, **24**, 110; (d) K. –I. Park, M. Lee, Y. Liu, S. Moon, G. –T. Hwang, G. Zhu, J. E. Kim, S. O. Kim, D. K. Kim, Z. L. Wang and K. J. Lee, *Adv. Mater.,* 2012, **24**, 2999; (e) D. –M. Shin, E. L. Tsege, S. H. Kang, W. Seung, S. W-. Kim, H. K. Kim, S. W. Hong and Y. –H. Hwang, *Nano Energy,* 2015, **12**, 268; (f) Z. L. Wang and J. Song, *Science*, 2006, **312**, 242.

3 (a) E. Fukada, *Q. Rev. Biophys.,* 1983, **16**, 59; (b) M. M. Jolandan and M. –F. Yu, *Biomacromolecules,* 2009, **10**, 2565.

4 (a) D. Farrar, K. Ren, D. Cheng, S. Kim, W. Moon, W. L. Wilson, J. E. West and S. M. Yu, *Adv. Mater.,* 2011, **23**, 3954; (b) A. Kholkin, N. Amdursky, I. Bdikin, E. Gazit and G. Rosenman, *ACS Nano,* 2010, **4**, 610.

5 B. Y. Lee, J. Zhang, C. Zueger, W. –J. Chung, S. Y. Yoo, E. Wang, J. Meyer, R. Ramesh and S. –W. Lee, *Nature Nanotech.,* 2012, **7**, 351.

6 M. M. –Jolandan and M. –F. Yu, *Nanotechnology,* 2009, **20**, 085706.

7 (a) P. –Y. Chen, X. Dang, M. T. Klug, J. Qi, N. –M. D. Courchesne, F. J. Burpo, N. Fang, P. T. Hammond and A. M. Belcher. *ACS Nano,* 2013, **7**, 6563; (b) C. K. Jeong, I. Kim, K. –I. Park, M. H. Oh, H. Paik, G. –T. Hwang, K. NO. Y. S. Nam and K. J. Lee, *ACS Nano,* 2013, **7**, 11016.

8 (a) Y. J. Lee, H. Yi, W. –J. Kim, K. Kang, D. S. Yun, M. S. Strano, G. Ceder and A. M. Belcher, *Science,* 2009, **324**, 1051; (b) Y. S. Nam, A. P. Magyar, D. Lee, J. –W. Kim, D. S. Yun, H. Park, T. S. Pollom, D. A. Weithz and A. M. Belcher, *Nature Nanotech.,* 2010, **5**, 340.

9 (a) J. –W. Oh. W. –J. Chung, K. Heo, H. –E. Jin, B. Y. Lee, E. Wang, C. Zueger, W. Wong, J. Meyer. C. Kim, S. –Y. Lee, W. –G. Kim, M. Zemla, M. Auer, A. Hexemer and S. W. Lee, *Nature Commun.,* 2014, **5**, 3043; (b) C. Mao, A. Liu and B. Cao, *Angew. Chem. Int. Ed.,* 2009, **48**, 6790.

10 (a) S. –W. Lee, C. Mao, C. E. Flynn and A. M. Belcher, *Science,* 2002, **296**, 892; (b) X. Dang, H. Yi, M. –Ho. Ham, J. Qi, D. S. Yun, R. Ladewski, M. S. Strano, P. T. Hammond and A. M. Belcher, *Nature Nanotech.,* 2011, **6**, 377; (c) D. Ghosh, Y. Lee, S. Thomas, A. G. Kohli, D. S. Yun, A. M. Belcher and K. A. Kelly, *Nature Nanotech.,* 2012, **7**, 677; (d) C. Mao, D. J. Solis, B. D. Reiss, S. T. Kottmann, R. Y. Sweeney, A. Hayhurst, G. Georgiou, B. Iverson and A. M. Belcher, *Science,* 2004, **303**, 213.

11 Y. Shi, S. He and J. E. Hearst, *J. Chem. Phys.,* 1996, **105**, 714.

12 Y. Wan, L. Xie, X. Zhang and Z. Zhong, *Appl. Phys. Lett.,* 2011, **98**, 122902.

13 J. Zhou, P. Fei, Y. Gu, W. Mai, Y. Gao, R. Yang, G. Bao and Z. L. Wang, *Nano Lett.,* 2008, **8**, 3973.

14 W. Lee and S. –J. Park, *Chem. Rev.,* 2014, **114**, 7487.

15 (a) G. –T. Hwang, H. Park, J. –H. Lee, S. Oh, K. –I. Park, M. Byun, H. Park, G. Ahn, C. K. Jeong, K. No, H. Kwon, S. –G. Lee, B. Joung and K. J. Lee, *Adv. Mater.,* 2014, **26**, 4880; (b) Q. Zheng, B. Shi, F. Fan, X. Wang, L. Yan, W. Yuan, S. Wang, H. Liu, Z. Li and Z. L. Wang, *Adv. Mater.,* 2014, **26**, 5851; (c) Z. L. Wang, G. Zhu, Y. Yang, S. Wang and C. Pan, *Mater. Today,* 2013, **15**, 532.

16 (a) X. Pu, L. Li, H. Song, C. Du, Z. Zhao, C. Jiang, G. Cao, W. Hu and Z. L. Wang, *Adv. Mater.,* 2015, **27**, 2472; (b) K. Y. Lee, M. K. Gupta and S. –W. Kim, *Nano Energy,* 2015, **14**, 139; (c) G. Zhu, P. Bai, J. Chen and Z. L. Wang, *Nano Energy,* 2013, **2**, 688.

